Histochemistry and Cell Biology (2021) 155:355–367
https://doi.org/10.1007/s00418-020-01936-z

ORIGINAL PAPER

Syndecan-3 contributes to the regulation of the microenvironment at the node of Ranvier following end-to-side neurorrhaphy: sodium image analysis

Chiung-Hui Liu[1,2] · Yu-Chen Kuo[1] · Che-Yu Wang[1] · Chao-Chun Hsu[1] · Ying-Jui Ho[3] · Yun-Chi Chiang[1] · Fu-Der Mai[4] · Wei-Jhih Lin[5] · Wen-Chieh Liao[1,2]

Accepted: 20 October 2020 / Published online: 10 November 2020

Abstract

Syndecan-3 (SDC3) and Syndecan-4 (SDC4) are distributed throughout the nervous system (NS) and are favourable factors in motor neuron development. They are also essential for regulation of neurite outgrowth in the CNS. However, their roles in the reconstruction of the nodes of Ranvier after peripheral nerve injury (PNI) are still unclear. Present study used an in vivo model of end-to-side neurorrhaphy (ESN) for 1–3 months. The recovery of neuromuscular function was evaluated by grooming test. Expression and co-localization of SDC3, SDC4, and Nav1.6 channel (Nav1.6) at regenerating axons were detected by proximity ligation assay and confocal microscopy after ESN. Time-of-flight secondary ion mass spectrometry was used for imaging ions distribution on tissue. Our data showed that the re-clustering of sodium and Nav1.6 at nodal regions of the regenerating nerve corresponded to the distribution of SDC3 after ESN. Furthermore, the re-establishment of sodium and Nav1.6 correlated with the recovery of muscle power 3 months after ESN. This study suggested syndecans may involve in stabilizing Nav1.6 and further modulate the distribution of sodium at nodal regions after remyelination. The efficiency of sodium re-clustering was improved by the assistance of anionic syndecan, resulting in a better functional repair of PNI.

Keywords Syndecan-3 · Syndecan-4 · Nerve regeneration · Nav1.6 · Sodium · End-to-side neurorrhaphy · Nerve regeneration · TOF–SIMS · Neurorrhaphy · Peripheral nerve injury · Ion

Abbreviations

SDC3	Syndecan-3
SDC4	Syndecan-4
CMAP	Compound muscle action potential
ESN	End-to-side neurorrhaphy
McN	Musculocutaneous nerve
UN	Ulnar nerve
TOF–SIMS	Time-of-flight secondary ion mass spectrometry
PNI	Peripheral nerve injury

Introduction

Peripheral nerve injury (PNI) is a common injury occurring when nerve axons undergo laceration or compression, resulting in disability and loss of sensation. In PNI cases, end-to-side neurorrhaphy (ESN) from the musculocutaneous nerve (McN) to the ulnar nerve (UN), is a frequently performed surgery to ensure the recovery of the injured nerve and to preserve the function of the donor nerve and

Electronic supplementary material The online version of this article (https://doi.org/10.1007/s00418-020-01936-z) contains supplementary material, which is available to authorized users.

✉ Wen-Chieh Liao
khrnangel@gmail.com

1 Department of Anatomy, Faculty of Medicine, Chung Shan Medical University, No. 110, Sec. 1, Jianguo N. Rd, Taichung 40201, Taiwan

2 Department of Medical Education, Chung Shan Medical University Hospital, No. 110, Sec.1, Jianguo N. Rd, Taichung 40201, Taiwan

3 Department of Psychology, Chung Shan Medical University, No. 110, Sec. 1, Jianguo N. Rd, Taichung 40201, Taiwan

4 Department of Biochemistry and Molecular Cell Biology, School of Medicine, College of Medicine, Taipei Medical University, No. 250, Wuxing St, Taipei 11031, Taiwan

5 Department of Forensic Science, Central Police University, 56 Shu-Jen Road, Kwei-San, Taoyuan 33304, Taiwan

the muscles it innervates. However, due to the structure difference between the donor nerve and the recipient nerve, mismatched components, including extracellular matrix (ECM), scaffold proteins, growth factors, and cells need to reorganize. These components of the recipient nerve conduit form a new microenvironment, where mediate axon sprouting and Schwann cell migration. Proteoglycans (PGs) are one of macromolecules of the ECM, which are composed by linear glycosaminoglycan (GAG) chains covalently linked to core proteins. PGs not only provide structural support of ECM, they also regulate neurites extension and ion channel arrangement during the development and regeneration of peripheral nerves (Gao et al. 2013; Gardiner 2017). Heparan sulphate proteoglycans (HSPGs) bear one to several heparan sulphate (HS) chains on the core proteins, which are suggested to promote tissue repair by facilitating important extracellular molecules binding and signalling, such as basic fibroblast growth factor (bFGF), glial cell-derived neurotrophic factor (GDNF), and vascular endothelial growth factor (VEGF) (Prince et al. 2010; Marquardt et al. 2015; Bespalov et al. 2011; Edwards and Hammarlund 2014; Mackenzie and Ruhrberg 2012).

The transmembrane protein syndecans have four subtypes (SDC1, SDC2, SDC3, and SDC4), which are classified as HSPG, because HS chains linked. In syndecan family, SDC3 and SDC4 are found abundantly expressed on the perinodal process of Schwann cells of the peripheral nervous system (PNS) (Goutebroze et al. 2003). The negative charged HS chains on syndecans are strongly bind water, ions, and positive charged proteins (Park 2018). Additionally, previous studies proposed that syndecans could act as co-receptors for various growth factors (Bernfield et al. 1993; Fukuda et al. 2018) and have crucial roles in the central nervous system (CNS) and PNS development (Hsueh and Sheng 1999). The expression levels of syndecans in nerve tissues can be regulated by matrix metallopeptidase 9 (MMP-9), a proteolytic enzyme secreted by Schwann cells that modulates nerve regeneration (Chattopadhyay and Shubayev 2009; Asundi et al. 2003). Aberrant expressions of SDC3 and SDC4 in CNS and PNS may cause nervous system disorders. It has been reported that SDC4 regulates the migration of tumor cells and neural crest cells (Matthews et al. 2008; Elfenbein and Simons 2013). Lack of the SDC3 may result in Charcot-Marie-Tooth disease, causing sensory and motor neuropathies that damage the peripheral nerves (Jordanova et al. 2003). SDC3 acts as a pleiotrophin (PTN) receptor, which was highly expressed by nigral dopaminergic neurons. Absence of SDC3 as the PTN receptor was associated with Parkinson disease (Marchionini et al. 2007).

The expression and re-distribution of voltage-gated sodium channels also play a crucial role in PNI (Henry et al. 2007). Sodium channels subtypes, Nav1.2 and Nav1.6 were found to assemble at the nodes of Ranvier, and Nav1.6 is the predominant channel subtype in the nodal region of mature neurons (Katz et al. 2018; Caldwell et al. 2000). According to previous studies, the expressions of syndecan-3, syndecan-4, and Nav1.6 were enriched in rat brain and peripheral nerve during development (Couchman 2003; Leterrier et al. 2010; Hsueh and Sheng 1999). We thus suggested that the distribution of Nav1.6 and sodium ion in the node of Ranvier may interact with SDC3 and SDC4, which involves action potential conduction in regenerating sprouts after PNI. The present study was to investigate changes in SDC3, SDC4, Nav1.6, and MMP-9 at the regenerating node of Ranvier by ESN rat model. Moreover, the time-of-flight secondary ion mass spectrometry (TOF–SIMS) was to measure the distribution and intensity of unlabelled sodium ions in tissue samples (Liu et al. 2016).

Materials and methods

Experimental animals

Young adult male Wistar rats weighing 200–300 g ($n = 32$) were obtained from the Laboratory Animal Center of the Chung Shan Medical University and were used in this study. All experimental animals were housed under similar conditions with controlled temperature and humidity. All experimental procedures with surgical intervention were approved by the Laboratory Animal Center Authorities of the Chung Shan Medical University (IACUC Approval No 1658).

Surgical procedures

The in vivo model of PNI was performed using end-to-side neurorrhaphy (ESN). Briefly, after the rats were deeply anaesthetized with an intraperitoneal injection of 7% chloral hydrate (Sigma-Aldrich, St. Louis, MO, USA), they were placed on a surgical microscope, and an incision was made along the left mid-clavicular line to expose the left brachial plexus. The musculocutaneous nerve (McN) was then transected at the margin of the pectoralis major muscle. The end of the proximal ulnar nerve (UN) was then neurorrhaphied to the side of the distal McN (Oberlin et al. 1994) with 10–0 nylon sutures (Ethilon, Edinburgh, UK) under the surgical microscope. The wound was closed with 5–0 silk, and the animals were monitored for 1–3 months after surgery. All operated animals were divided into three groups. A sham operation was performed in Group I by simply exposing the brachial plexus. Group II (ES1M group) and Group III (ES3M group) were treated with end-to-side neurorrhaphy for 1 and 3 months, respectively. The number of animal used for the following assays is listed in Table 1.

Table 1 Experimental design for animal study

Types of examinations*	Groups and number of animal
RNA extraction and RNA sequence	Sham-op group ($n=3$)
	ES1M group ($n=3$)
Fresh tissues for Western blotting	Sham-op group ($n=3$)
	ES1M group ($n=5$)
	ES3M group ($n=5$)
Serial cryostat sections for:	
1. Immunofluorescence stain	Sham-op group ($n=3$)
2. Proximity ligation assay	ES1M group ($n=5$)
3. Time-of-flight secondary ion mass spectrometry	ES3M group ($n=5$)

*All animals were applied to sticker removal grooming test and compound muscle action potential recording before sacrifice

Perfusion and tissue preparation

For quantitative morphological analysis and TOF–SIMS, half amounts of rats from all experimental groups were deeply anesthetized with 7% chloral hydrate (0.4 mL/100 g) and subjected to transcardiac perfusion with 100 mL of Ringer's solution, followed by 45 min of fixation with 4% paraformaldehyde in 0.1 M phosphate buffer (PB), pH 7.4. After perfusion, the repaired nerve were removed and kept in a similar fixative for 2 h. The tissue block was then immersed in graded concentrations of sucrose buffer (10–30%) for cryoprotection at 4 °C overnight. Serial 25-µm-thick sections of the nerve segment muscle were cut longitudinally with a cryostat (CM3050S; Leica Microsystems, Wetzlar, Germany) on the following day. Every sixth nerve sections were selected from each animal and processed for immunostaining and proximity ligation assay (PLA) assay, and TOF–SIMS. For immunoblotting, another half of the ESN animals deeply anesthetized were perfused with Ringer's solution, and then, the musculocutaneus nerve was quickly removed under a dissecting microscope. The samples were stored at −80 °C until use.

Sticker removal grooming test and compound muscle action potential recording

Sticker removal grooming test was performed to evaluate the functional recovery of ESN rats before CMAP recording (Liao et al. 2013). Time spent on removing a standard-size sticker (5 cm in length and 0.5 cm in width) from ipsilateral ear was recorded in sham-op, ES1M, and ES3M rats. To monitor the functional status of a motor unit pool in ESN rats, the measurement of CMAPs from the brachial plexus nerve using needle electrodes was applied here. CMAPs in the repaired nerve and target muscle were recorded using a Power Lab electromyogram (AD instrument, Sydney, Australia). For recording, a silver stimulating electrode was placed under the reconnection site and a silver recording electrode was inserted into the biceps brachii muscle at the mid-humeral level. A 5–0 nylon suture was applied at a 1 cm distance between the recording and stimulating electrodes. The animal's tail was connected to the signal ground line. A current of 5 mA with 0.2 ms square pulse at a repetition of 0.2 Hz was applied. Results were recorded digitally and the response amplitudes analyzed.

Nav1.6, syndecan-3 and syndecan-4 immunofluorescence stain

For Nav1.6, syndecan-3 and syndecan-4 immunohistochemistry, the collected tissue sections were first placed in a blocking medium containing 0.1% triton X-100, 3% normal goat serum, and 2% bovine serum albumin (all from Sigma-Aldrich, St. Louis, MO, USA) for 1 h to block nonspecific binding. After several washes in phosphate-buffered saline (PBS), the sections were incubated in mouse anti-Nav1.6 antibody (Scn8a antibody MAB11980; 1:1000, Abnova Corporation, Taipei, Taiwan), rabbit polyclonal anti-syndecan-3 antibody (tcfa8417; 1: 500, Taiclone, Taipei, Taiwan), and rabbit polyclonal anti-syndecan-4 antibody (ARG20194; 1: 500, Arigo biolaboratories, Hsinchu, Taiwan) with the blocking medium for 24 h at 4 °C. Negative controls were performed by replacing primary antibodies with an isotype-matched control IgG (Jackson Immuno-Research, West Grove, PA, USA) at the same concentration. After incubation in primary antibodies, the sections were further incubated with Alexa Fluor anti-mouse IgG (1:200, Jackson Immuno- Research, West Grove, PA, USA) and Cy3-conjugated anti-rabbit IgG (1:200, Jackson Immuno-Research, West Grove, PA, USA) for 1 h. All mounted sections were examined and photomicrographed under a confocal fluorescence microscope (SP8X, Leica Microsystems, Wetzlar, Germany). The Z-stacked confocal images of the nerve were captured with a confocal microscope to analyze the Nav1.6, syndecan-3 and syndecan-4 distribution and recovery of the repaired nerve. Each confocal photomicrograph is created using a stacked series of scans of a nerve section (25 µm in total thickness). The z-stack images were captured from regenerating axons (5 µm optical slice thickness, 10 z-sections collected at 0.486-µm intervals).

RNA extraction and screening differential gene expression in ESN Rats

Total RNA was extracted from 100 mg of rat nerve tissue using TRIzol reagent (Invitrogen), and 1 µg of RNA was reverse transcribed using a PrimeScript™ RT Reagent Kit (TaKaRa). The cDNA was subjected to real-time PCR. Real-Time PCR System (Bio-Rad, RNA sequence (RNA-seq)

will performed by Genomicsco, Taiwan on sham-operation (sham-op) tissue ($n=3$) and ESN-1 M tissue ($n=3$) (Garber et al. 2011; Wang et al. 2017). Expression of interesting genes will be confirmed by Western blots. The important findings of signaling pathways will be further confirmed by Western blots.

Western blotting

Musculocutaneous nerve tissue samples were subjected to western blot analysis. Three tissue samples of distal McN removed from the suture site of each group was first homogenized with Kaplan buffer (50 mM Tris buffer, pH = 7.4, 150 mM NaCl, 10% glycerol, 1% NP40, and protease inhibitor cocktail) and then clarified by centrifugation. Then, equal amounts of solubilized proteins and cell lysates were separated on SDS-PAGE (8%) and electroblotted onto nitrocellulose membranes (Bio-Rad Laboratories, Hercules, CA, USA). The membranes were then blocked with 5% skim milk and probed with antibodies against β-actin (1:10,000, BD Biosciences, San Jose, CA,USA), Nav1.6 (1:1000, Abnova Corporation, Cambridge, UK), MMP-9 (1:1000; proteintech, Chicago, USA), syndecan-3 (1:500, Taiclone), and syndecan-4 (1: 500, Arigo Biolaboratories Corp., Hsinchu, Taiwan) at 4 °C overnight. After incubation with primary antibodies, the membranes were incubated with horseradish peroxidase-conjugated secondary antibodies (Bethyl Laboratories, Montgomery, TX, USA) at a dilution of 1:10,000 for 1 h at room temperature. ECL solutions (Millipore, Temecula, CA, USA) were used to detect the signals generated and the intensity of bands was analyzed by image J software.

Proximity ligation assay

The proximity ligation analysis (PLA) experiment was showing the interaction between syndecan-3 and Nav1.6 channel (Clausen et al. 2016). The nerve tissue was blocked in Duolink blocking solution (Sigma-Aldrich, St. Louis, MO, USA). The tissues were then stained with primary antibodies together with syndecan-3 and syndecan-4 (1: 500, Taiclone, Taipei, Taiwan) or Nav1.6 (1:1000, Abcam, Cambridge, UK) overnight in these concentrations. After several washes in wash buffer A (DUO82047), the tissues were then stained with duolink In Situ PLA probe anti-mouse minus (DUO92004) and duolink In Situ PLA Probe anti-rabbit plus (DUO92002) diluted in antibody diluent (DUO82008). The tissues were then treated with the ligation solution, followed by incubation with the amplification solution. The sections were finally washed with wash buffer B (DUO82048). Slides were mounted using Duolink In Situ mounting medium with hoechst33342.

Time-of-flight secondary ion mass spectrometry (TOF–SIMS) analysis

TOF–SIMS analysis was carried out on a TOF–SIMS IV in strument (ION-TOF GmbH, Munster, Germany) as described in our previous studies (Liu et al. 2016). Serial sections were observed and images of them captured by differential interference contrast (DIC) microscopy (Axioskop 2 plus, Zeiss, Göttingen, Germany). A gallium (Ga^+) ion gun operated at 25 kV was used as the primary ion source (1 pA pulse current) for experiments conducted during this study. The Ga^+ primary ion beam scanned an area of 100 μm^2. Positive secondary ions passing through a reflectron mass spectrometer were detected with a micro-channel plate assembly operating at 10 kV postacceleration. Mass calibration of the ion spectrum was achieved using a set of mass peaks such as m/z = 15 ($CH3^+$), 41 ($C3H5^+$), and 69 (Ga^+), and a paraformaldehyde molecule, since this element was the major component in the tissue matrix following vascular fixation (Liu et al. 2017). The ions related to Na^+ ($m/z=23$) were used to identify and evaluate the molecular image of potassium expression.

Statistical analysis

For TOF–SIMS analysis, the spectral intensity detected from each section was normalized to the ion intensity of paraformaldehyde (serving as base line = 100%) and was expressed as the percentage above the base line. All quantitative data acquired from spectrometry, immunofluorescence, and immunoblotting in sham-op and ESN rats were subjected to one-way ANOVA followed by Bonferroni post-hoc test. Data were presented as the mean ± SD. $P<0.05$ was considered statistically significant.

Results

Expression of syndecans, Nav1.6 and MMP-9 after end-to-side neurorrhaphy

The clusterization of sodium channels at the node of Ranvier is known to be essential in saltatory conduction of the axon. When nerve injury occurs, the expression level of syndecans and sodium channels might be altered. To study gene expression changes in injured nerves, RNA-seq was performed 1 month following ESN. The relative degree of genes expressions of ES1M group compared to that of the sham-op group was displayed through the dot plot (Fig. 1a). The result shows significant upregulation of *SDC3*, *SDC4*, *Scn8* (Nav1.6), and *MMP-9* in 1 month after ESN surgery nerve tissue. Expression of *SDC3* and *SDC4* in the ES1M group were approximately two-fold higher than that in the

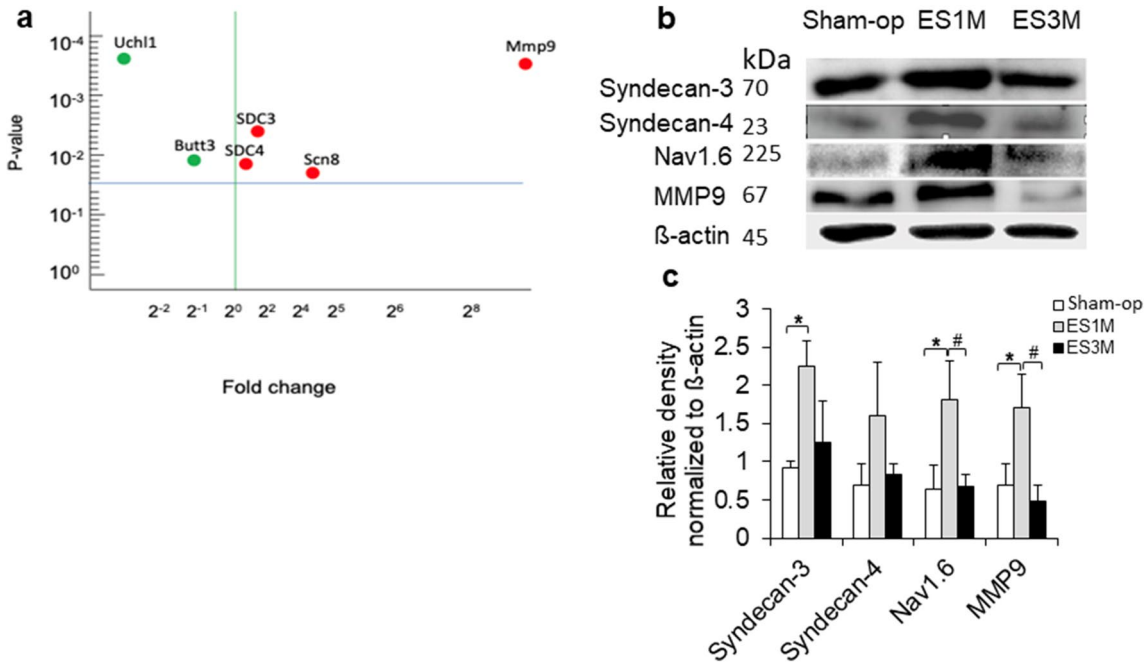

Fig. 1 Diagram illustrated the gene and protein expression in nerve tissues of normal and 1- to 3-month EEN rats. Dot plot (**a**) displayed the relative expression quantity of selected genes of ES1M group compared to that of sham-op group 1 month after ESN. Significant upregulation of syndecan-3 (SDC3 gene), syndecan-4 (SDC4 gene), Nav1.6 (Scn8 gene), MMP-9, Uchl1 (PGP9.5 gene), and Butt3 (ß3-tubulin gene) are shown by red dot. Fold change represents the ratio of ES1M group to sham-op group. Immunoblot (**b**) showing syndecan and Nav1.6 expressions in nerve tissues of normal and 1–3-month ESN rats. Expressions of syndecan-3, syndecan-4, Nav1.6, and MMP-9 were detected. β-actin was used as a loading control. Densitometric analysis (**c**) indicates a relatively higher expression of each protein in the ES1M compare to the sham-op groups. Average ± SD from three experiments was shown. Note that the expression of each protein increased 1-month following ESN. Data are present as mean ± SD from three independent experiments. $^{*}P < 0.05$ compared to sham-op group. $^{\#}P < 0.05$ compared to ES1M group

sham-op group, while *MMP-9* showed a greater than 256-fold increase in expression. To confirm the increased levels of proteins mentioned above, we further quantified the expression of each protein on regenerating axons using western blots. In consistently, the protein expression of SDC3, SDC4, Nav1.6, and MMP-9 are increased in 1 month after ESN. The protein levels of syndecan-3, Nav1.6, MMP-9, andsyndecan-4 in the ES1M rats were 2.43-fold, 2.8-fold, and 1.42-fold, and 2.28-fold more than that of the sham-op group, respectively. After 3 months of ESN, the expression of syndecan-3 and syndecan-4 were still slightly higher in the ES1M group than in the sham-op group (Fig. 1b, c). It may result from an increase in the remodelling of new sprouts. In addition, the expressions of Nav1.6 and MMP-9 were reduced compare to that in the 1-month ESN tissue.

Functional recovery after end to side neurorrhaphy

To evaluate the functional recovery of injured nerves, we conducted sticker removal grooming test on sham-op, ES1M, and ES3M groups. The respond time for removing the sticker placed on the ipsilateral ear was recorded. The average time for the sham-op group to remove the sticker was less than a second. One month after ESN, the time needed escalated significantly to an average of 5.0 ± 0.9 s. The performance was slightly recovered 3 months after ESN, indicated by $^{*}P < 0.05$ compare to ES1M group, with an average of 2.1 ± 0.6 s (Fig. 2a).

To confirm that the clusterization of Nav1.6 in nodal regions correspond with nerve conduction, we further examine the action potential of regenerating nerves using CMAP analysis. The responses were recorded from biceps brachii muscle upon activation of the nerve. According to electrophysiological recordings, the ES1M groups generated low amplitude and long duration action potentials in comparison to sham-op group.

Follow-up immediately, at 3 months after ESN demonstrated that motor function was gradually restored and generated CMAPs with amplitude similar to sham-op group (6.96 ± 0.05 mV in sham-op, 4.20 ± 0.08 mV in ES1M, and 7.00 ± 0.10 mV in ES3M group). In addition, the duration of ES1M group (9.66 ± 1.52 ms) and ES3M group (10.0 ± 0.81 ms) increased significantly, $^{*}P < 0.05$ compares to sham-op group (5.33 ± 0.57 ms) (Fig. 2b, c). CMAP duration may specifically detect these detail changes of insufficient axonal regeneration.

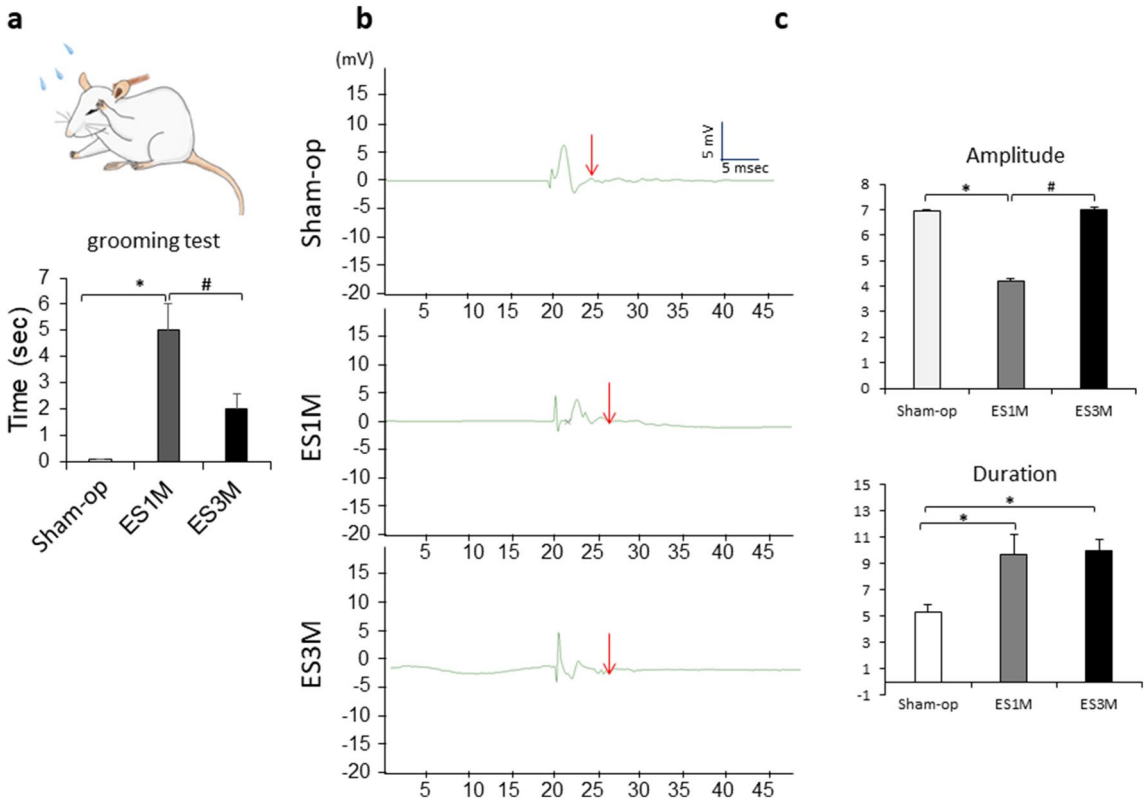

Fig. 2 Sticker removal grooming test and compound muscle action potentials (CMAPs) were performed to evaluate the functional recovery of ESN rats. **a** Schematic demonstrates the sticker removal grooming test assessing the time spent in sticker removing of sham-op rats and ESN rats. Response time for removing a sticker placed on the ipsilateral ear was recorded. The results were from sham-op rats, ES1M rats, and ES3M rats. Note that the performance was partly recovered in ES3M rats. $n = 10$ for each group. Data were shown as the mean ± SD. $^{*}P < 0.05$ compared to the corresponding sham-op rats. $^{\#}P < 0.05$ compared to the corresponding ES1M rats. **b** The recovery of CMAPs after ESN. The responses were recorded from biceps brachii muscle upon activation of the nerve. The representative responses recorded from the sham-op group (upper row) and 1- and 3-month (lower rows) following end-to-side neurorrhaphy are illustrated. The arrow indicates the end of the duration. Stimuli at moderate (5 mA) strengths were applied to the nerve above the neurorrhaphy site. Histograms (**c**) show the averages of amplitude and duration, respectively. $n = 10$ for each group. Values are the mean ± SD. $^{*}P < 0.05$ compared to that of sham-op value. $^{\#}P < 0.05$ compared to the corresponding ES1M rats

Distribution of syndecans and Nav1.6 in longitudinally regenerating axon after end-to-side neurorrhaphy

To examine the distribution of syndecan-3, syndecan-4 and Nav1.6 in ESN model, the distal ends of the regenerating axons were immunostained with anti-syndecan-3, anti-syndecan-4, and anti-Nav1.6 antibody 1–3-month post-surgery. Confocal microscopy revealed that in the sham-op group, syndecan-3 and Nav1.6 were concentrated at the node of Ranvier, whereas syndecan-3 and Nav1.6 were widespread throughout the regenerating nerve fiber in the ES1M group. Three months after ESN, syndecan-3 and Nav1.6 congregated and gathered around the nodal region again (Fig. 3). The nerve bundles were still smaller in ES3M rats as compared of that of sham-op group. Similarly, syndecan-4 clustered at the paranodal region, adjacent to Nav1.6 that is located in the node of Ranvier in sham-op group. One-month post-surgery, syndecan-4 was enriched in proliferative Schwann cell. Meanwhile, Nav1.6 scattered across the regenerating axons rarely co-localized with syndecan-4, the distribution of syndecan-4 resumed to the pattern similar to that of the sham-op group 3 months following ESN (Fig. 4).

To further verify the interaction between syndecan-3/4 and Nav1.6 in regenerating axons, we investigated the co-localization of both proteins by proximity ligation assay. The recipient nerve tissues were stained with Duolink In-Situ PLA Probes 1- and 3-month following ESN. The number of signals in sham-op group was abundant, whereas it decreased in ES1M and ES3M groups (Fig. 5a). Quantification of the PLA analysis shows an average number of syndecan-3/Nav1.6 linked signals of 10 ± 4 /100 μm^2 in sham-op group, and an average number of 3 ± 2 /100 μm^2 and 5 ± 3 /100 μm^2 in the ES1M and ES3M groups, respectively (Fig. 5b). In

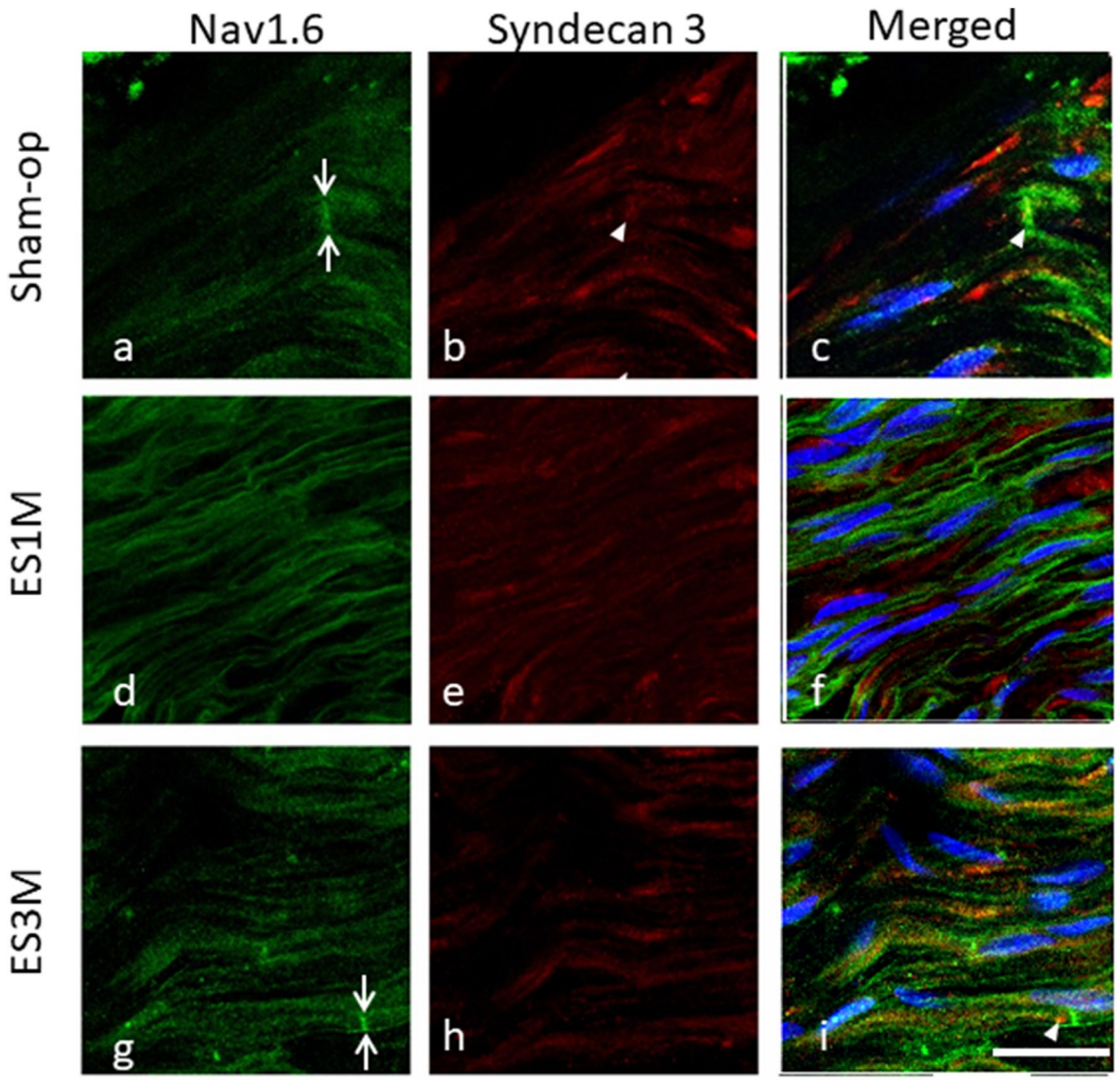

Fig. 3 Confocal photomicrographs showing the distribution of Nav1.6 and syndecan-3 expression in regenerating axons. The recipient nerve tissue (distal end of McN) was immunostained with anti-Nav1.6 antibody (green) and anti-syndecan-3 antibody (red) 1- and 3-month following ESN. After the labelling of sections, nuclei DNA were counterstained with Hoechst33342 (blue). Nav1.6 channels clustered at the node of Ranvier, colocalizing with syndecan-3 (**a**, **b**, **c**), whereas they scattered throughout the regenerating nerve fiber 1 month after ESN (**d**, **e**, **f**). Note that Nav1.6 channels underwent structural rearrangement at the nodal region accompanied with syndecan-3 3-month following ESN (**g**, **h**, **i**). Scale bar = 25 µm

contrast, much less syndecan-4 / Nav1.6 linked signals were observed, and no significant change in the sham-op group and ES1M group (signal: 2.3 ± 1.0 /100 µm^2 in sham-op group, 2.6 ± 1.2 /100 µm^2 in ES-1 M group, 1.0 ± 0.3 /100 µm^2 in ES-3 M group). These data suggests that syndecan-3 was closely co-localized with Nav1.6 in the sham-op group, while the co-localization was significantly decreased 1 month after surgery and gradually recovered after 3 months.

Sodium ion mapping at the node of Ranvier after ESN by time-of-flight secondary-ion mass spectrometry

It is known that the sulphated proteoglycan chains of syndecans are negatively charged, serving as a cationic pool to congregate ions on nerve axons (Susuki et al. 2013). To evaluate the distribution of sodium ion on the regenerating axons, we analyzed nerve tissues by TOF–SIMS.

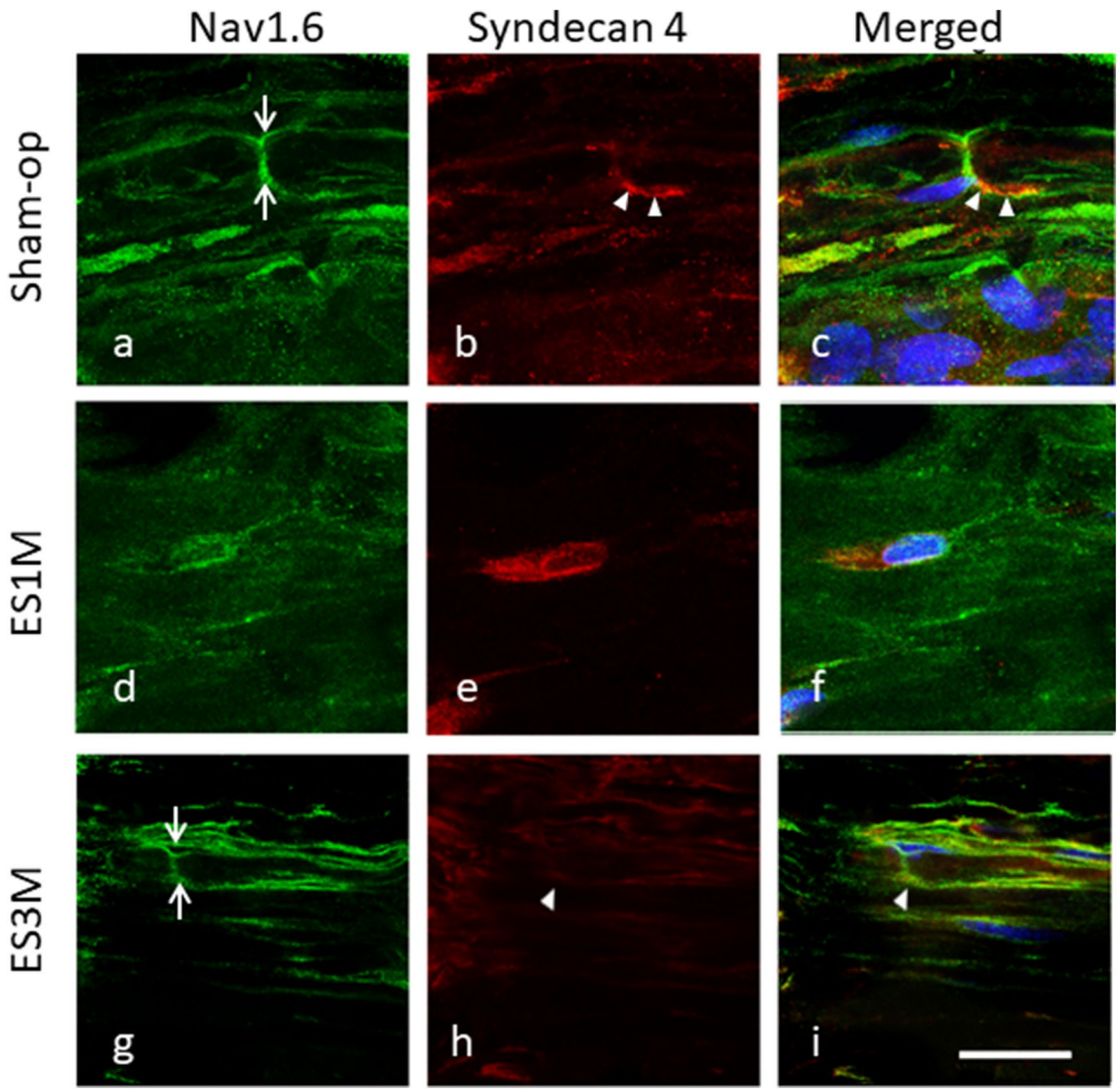

Fig. 4 Confocal microphotographs showing the distribution of Nav1.6 and syndecan-4 expression in regenerating axons. The recipient nerve tissue (distal end of McN) was immunostained with anti-Nav1.6 antibody (green) and anti-syndecan-4 antibody (red) 1- and 3-month following ESN. After the labelling of sections, nuclei DNA were counterstained with Hoechst33342 (blue). Nav1.6 channels clustered at the node of Ranvier, colocalizing with syndecan-4 (**a**, **b**, **c**), whereas they scattered throughout the regenerating nerve fiber 1-month following ESN (**d**, **e**, **f**). Note that Nav1.6 channels underwent structural rearrangement at the nodal region accompanied with syndecan-4 3-month following ESN (**g**, **h**, **i**). Scale bar = 25 µm

TOF–SIMS showed the ionic images of sodium distribution as well as the normalized spectral intensity of sodium ions on tissue slides. The results showed that strong sodium ion signals were concentrated at the node of Ranvier in the sham-operation axons (Fig. 6a). One month following ESN, the sodium ion signals decreased significantly. Instead of concentrating at the node of Ranvier, sodium ion signals were found to disperse along the axons. At 3-month following ESN, most of the sodium ions assembled at the node of Ranvier again. This result revealed a re-establishment of sodium ions distribution on regenerating axons during the recovery process after ESN. The absolute counts of sodium ions on the nerve tissue were normalized to the total paraformaldehyde ions. We found that the quantity of sodium ions significantly decreased 1 month after ESN and then increased to equivalent levels relative to the sham-operation group at 3 months (Fig. 6b, c).

Discussion

In this current study, the differential expressed genes 1 month after ESN were identified by RNAseq, and we focus on the expression of syndecan-3/4, sodium channels, and

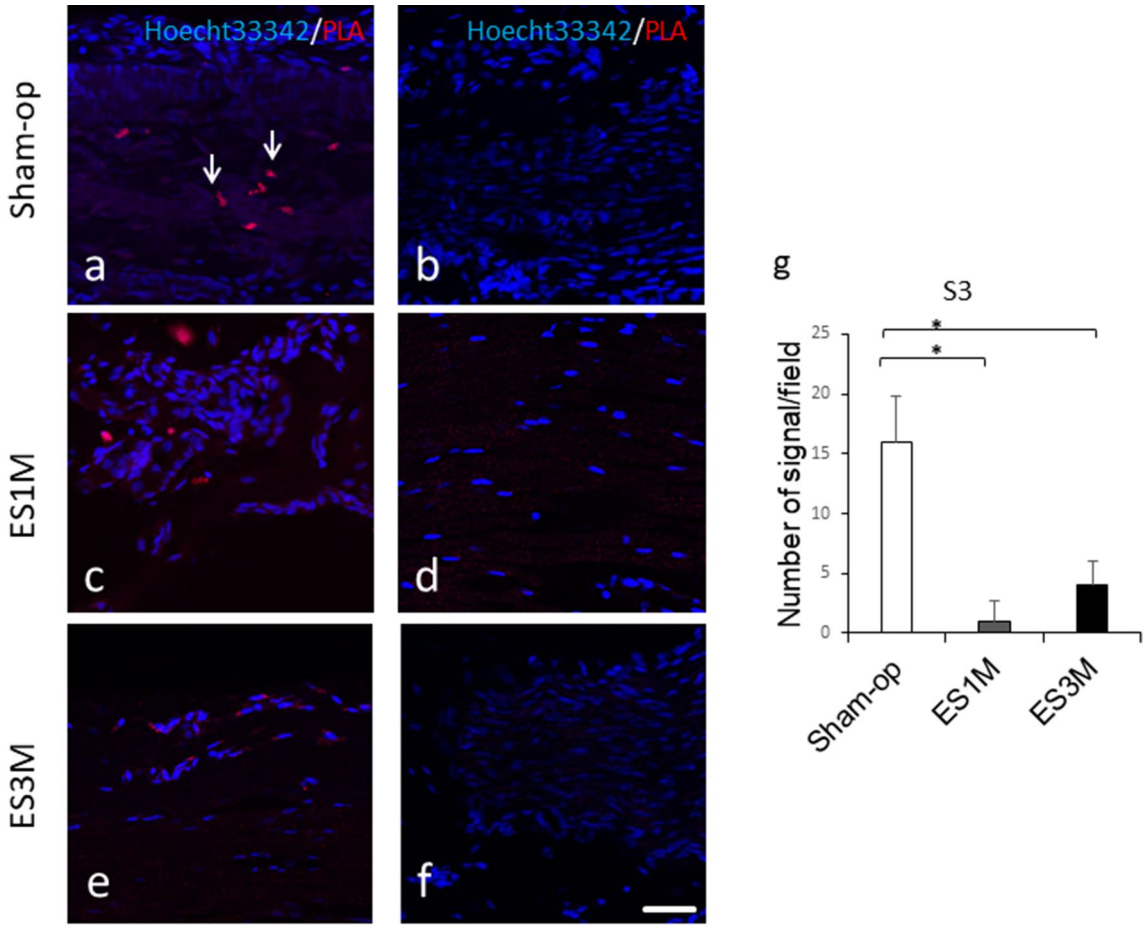

Fig. 5 Proximity Ligation Assay (PLA) showing colocalization between syndecan-3 and Nav1.6 channels. **a** The recipient nerve tissue was stained with Duolink In Situ PLA Probe antibodies 1- and 3-month following ESN. Fluorescence signal (red) indicates ligation signal of syndecan-3/Nav1.6 (**a**, **c**, and **e**) and signal of syndecan-4/Nav1.6 (**b**, **d**, and **f**). After the labelling of sections, nuclei DNA were counterstained with Hoechst33342 (blue). Please note that the PLA signals (indicated by the arrows) were much more in the sham-op group when compared to that of ES1M group and ES3M group. In the nerve tissue of sham-op (panel b) ES1M (panel d) and ES3M (panel f) group, which were lacking PLA signal of syndecan-4/Nav1.6. Scale bar = 50 µm. **g** Quantification of the PLA analysis. Significant decrease of syndecan-3/Nav1.6 signals in ES1M and ES3M are indicated by $*P < 0.05$. Vales are mean ± SD

MMP-9 in regenerating axons. These proteins were upregulated 1 month after ESN, and declined 3-month post-surgery. PLA analysis revealed that syndecan-3 but not syndecan-4 are closely co-localized with Nav1.6 channels in the nodal region of the axons in normal condition. The co-localization of syndecan-3 and Nav1.6 in the nodal region drastically decreased 1 month after ESN and gradually reappeared in 3 months, that is associated with the functional recovery of nodal reformation that regulated by Nav1.6 recluster (Fig. 7).

As the regenerating process begins, our study indicates an upsurge in MMP-9 1 month after neurorrhaphy. MMP-9 as well as a mitogen-promoted Schwann cell proliferation, supported remyelination of axons and activated cell migration (Kim et al. 2012; Dufour et al. 2010). By degrading the major barrier in the peripheral nerves such as chondroitin sulphate proteoglycan (CSPG), MMP-9 clears a path for neurite outgrowth (Ferguson and Muir 2000). Proliferative Schwann cells migrate to the repair site creating a microenvironment abundant in proteoglycans achieve maintaining axo-glial interaction and nerve regeneration (Quintes et al. 2010; Schlosshauer et al. 2003). Meanwhile, excessive syndecan-3 was secreted by Schwann cells. The heparan sulfate (HS) chains on syndecan-3 are able to capture various growth factors, such as glial cell line-derived neurotrophic factor (GDNF) (Webber and Zochodne 2010; Bespalov et al. 2011), and facilitate Schwann cells proliferation and migration. Since MMP-9 has be reported to shred transmembrane syndecans into free ectodomain (Manon-Jensen et al. 2010), the up-regulation of MMP-9 in our ESN model may also result in the accumulation of syndecans ectodomain to trap growth factors in the regenerating microenvironment.

At the late stages of peripheral nerve regeneration, the sprouting axons began to be myelinated by Schwann cells, and the gaps between myelin sheaths formed the node of

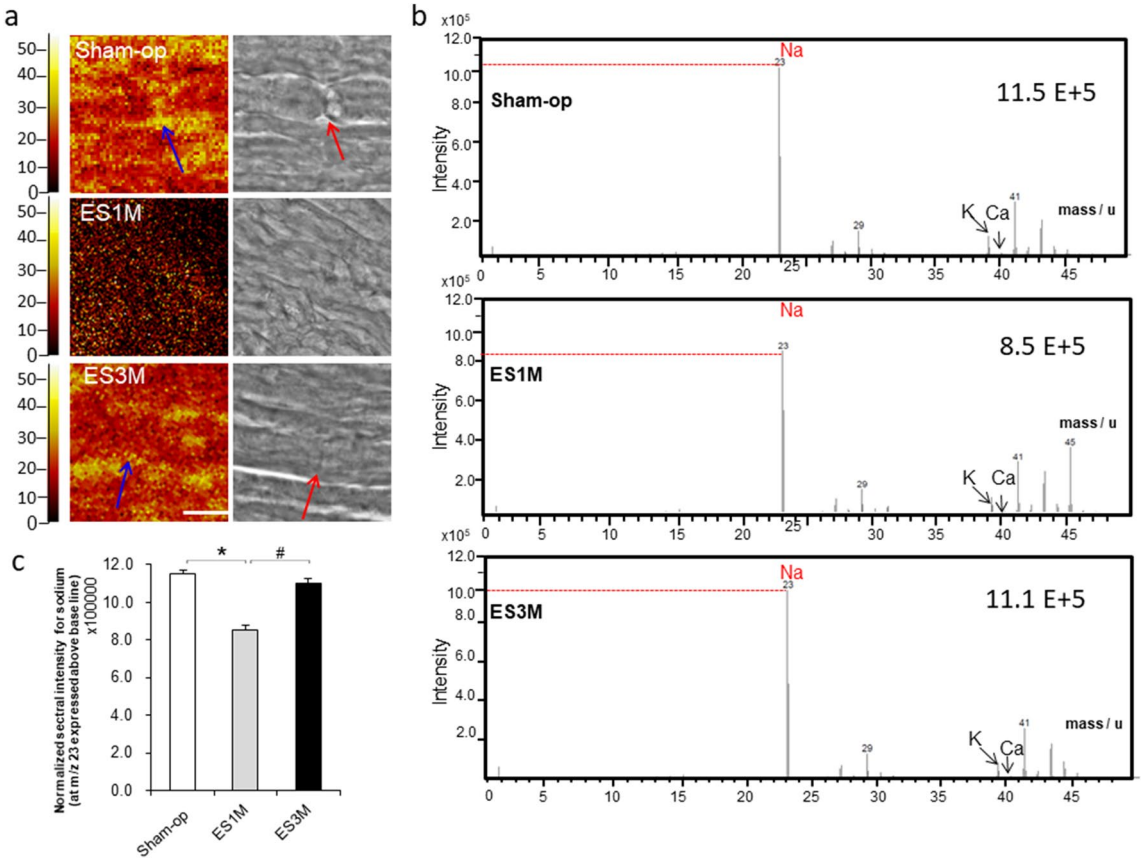

Fig. 6 TOF–SIMS images of regenerating axons. **a** Ionic images of sodium (left column) and corresponding DIC bright filed images (right column) on the serials longitudinal sections of repaired nerve from sham operation (sham-op), 1 and 3 months after ESN groups were shown. The ionic imaging of Na^+ signaling is expressed by a color scale in which bright colors represent high levels of Na^+ (m/z 23, the color scale: ion counts). Blue arrows indicate sodium-concentrated spots on the node of Ranvier, and red arrows indicate the location of spots on DIC images. Note that sodium-concentrated spots appeared segmentally at the node of Ranvier of the sham-op group, dispersed in the ES1M group, and partly re-clustered in ES3M group. Representative photographs are shown. Scale bar = 100 µm. **b** TOF–SIMS positive spectra (from 1 to 50 m/z) of sham-op, ES1M, and ES3M are shown. In sham-op rats, strong sodium intensity with significant sodium ionic localization was detected in the node of Ranvier of sham-op group. Following ESN, the Na^+ intensity was drastically decreased at 1 month, and recovery at 3 month after ESN. **c** The nerve sections revealed the intensity of sodium (m/z 23) after normalization to the total paraformaldehyde ions of each analysis. The spectral intensity for normalization was similar among numerous experimental groups. Note that normalized Na^+ intensity decreased in the ES1M group and recovered in the ES3M group. $N = 10$ for each group. $^*P < 0.05$

Ranvier. During PNS node formation, our study showed that syndecan-3 and syndecan-4 were mainly found in the node of Ranvier. Congregated at the node of Ranvier, syndecans linked to anchor proteins and were known for stabilizing the distribution of ion channels (Mitsou et al. 2017; Marquardt et al. 2015), and accumulation of Nav1.6 channels and sodium at nodes of Ranvier is paramount for action potential. Comparing to the distribution of Nav1.6 channels and syndecan-3/4 at nodes of Ranvier, we observed that the syndecan-4 seems more predominantly located at the para-nodal region, while syndecan-3 and Nav1.6 channels located at nodal region. Our PLA assays were further confirmed this observation and imply the distinct functions of syndecan-3 and syndecan-4 at nodes of Ranvier.

During the process of nerve regeneration, the syndecan-3/4 and Nav1.6 were re-expression and re-distribution. We found the up-regulation of syndecan-3/4 in ESN-1 M tissue by RNAseq and western blots. We observed the scattered Nav1.6 channels were less co-localized with syndecan-3 in the ESN-1 M group, whereas the level of sodium decreased on the nerve tissue. In the ESN-3M tissue, the co-localization of Nav1.6 and syndecan-3 obvious increased. Thus, these evidence pointed that syndecan-3 has a more important role than syndecan-4 in stabilizing sodium channels in peripheral nerve axons. Previous study proposed that syndecan-3 contained five extracellular GAG attachment sites which is more than that of syndecan-4 (Sarrazin et al. 2011). These GAG chains may endorse the functions syndecan-3 during the nerve regeneration.

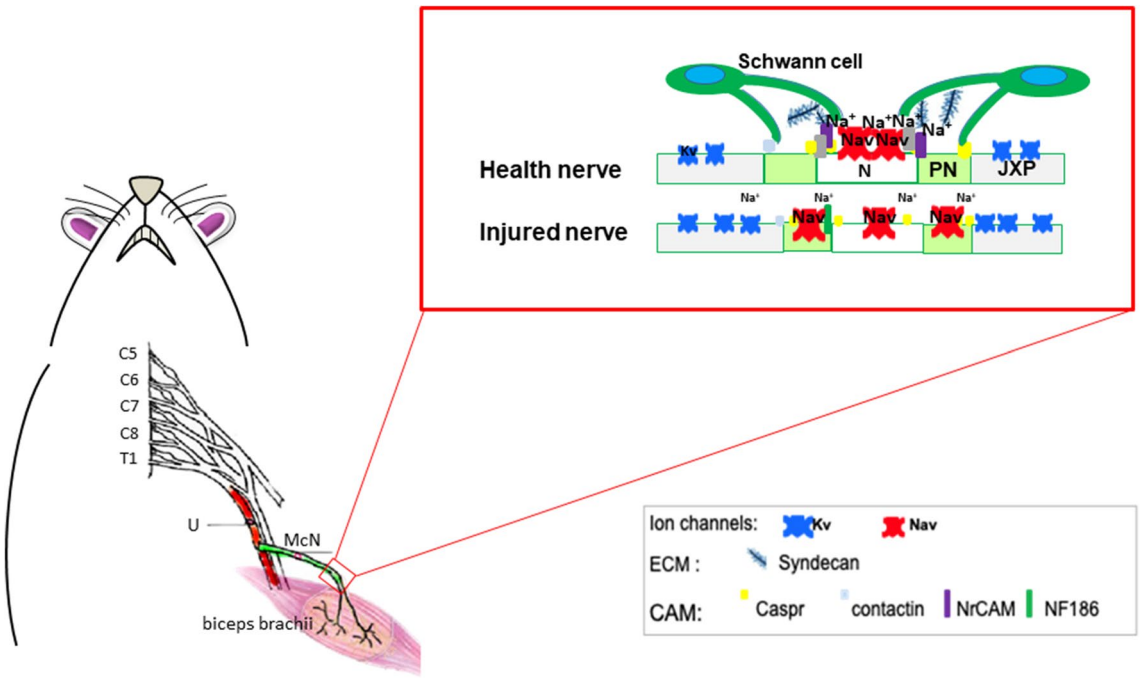

Fig. 7 Schematic illustration of end-to-side neurorrhaphy of musculocutaneous nerve (McN) to ulnar nerve (U). The red rectangle showed syndecan-3 and Nav1.6 interaction for sodium attraction in the recipient nerve. The node of Ranvier has high density of Nav1.6 channel which are co-localized with syndecan-3. Nerve injury resulted in syndecan-3 and Nav1.6 that dispersed along the axons. Nodes of Ranvier reformation occurs after ESN, thereby syndecans-3 attracting Na^+ aggregation and increasing the local concentration of Na^+ at the nodal region. Axonal domains: node of Ranvier (N), paranode (PN), and juxtaparanode (JXP)

To verify if the recovery of ion distribution correlated with the node of Ranvier, where syndecan-3 located, we performed TOF–SIMS to observe the disposal of ions in different phases of sprouting axons. And we focused on the sodium signals in the nodal region, since sodium is the major ion that triggers action potentials. The results exhibited that the intensity of sodium decreased in the ES1M group, owing to Nav1.6 dispersed and not yet formed in the node of Ranvier. Three months after ESN, highly rich sodium gathered at the nodal region with the amount similar to sham-operation groups. This provides evidence of a successful recovery on both ion channel distribution and node of Ranvier formation. Previous studies showed that syndecan-3 is localized on Schwann cell processes that participate in the nodal formation and are considered to serve as a cationic pool through the highly negatively charged heparin sulphate (Susuki et al. 2013; Meneghetti et al. 2015; Coulson-Thomas 2016). These results correspond to our TOF–SIMS analysis in which redistributed Na^+ concentrated and reclustered within a syndecan-3/Nav1.6 co-localized area of the ESN-3 M rats.

Conclusion

The primary findings of our study suggested that the functions of syndecan-3 are critical in Nav1.6 distribution at the node of Ranvier during peripheral nerve regeneration. In addition to binding anchor proteins and stabilizing Nav1.6, the negatively charged GAG chains of syndecan-3 can also attract cations, recruiting more sodium around the sodium channel (Fig. 7). This results in larger action potentials triggering and better functional recovery. Our results will not only improve our understanding of syndecan-3, syndecan-4 and Nav1.6 in the initial stage of nerve regeneration but will also provide insights into syndecan-3 targeting drugs in the late stages of PNS node reformation for clinical usage.

Acknowledgements This study was supported by research grants to Dr. Wen-Chieh Liao and Dr. Chiung-Hui Liu from the Ministry of Science and Technology, Taiwan, (MOST-108-2320-B-040-013-, 109-2320-B-040-009-, and 109-2320-B-040-007-MY3). Cryostatting (CM3050S, Leica 149 Microsystems) was performed in the Instrument Center of Chung Shan Medical University, which was supported by Ministry

of Science and Technology, Ministry of Education, and Chung Shan Medical University.

Author contributions Chiung-hui Liu and Yu-chen Kuo conceived of the study, performed image analysis; and participated in the redaction of the manuscript. Che-Wu Wan and Chao-Chun Hsug carried out immunobloots on nerve tissue. Ying-Jui Ho and Yun-Chi Chiang performed immunocytochemistry experiments on repaired nerves. Fu-Der Mai and Wei-Jhih Lin participated in the TOF–SIMS analysis. Wen-Chieh, Liao participated in the design and coordination of the study, and drafted the manuscript. All authors read and approved the manuscript.

Compliance with ethical standards

Conflict of interest The authors have declared that no conflict of interest exists.

References

Asundi VK, Erdman R, Stahl RC, Carey DJ (2003) Matrix metalloproteinase-dependent shedding of syndecan-3, a transmembrane heparan sulfate proteoglycan Schwann cells. J Neurosci Res 73(5):593–602. https://doi.org/10.1002/jnr.10699

Bernfield M, Hinkes MT, Gallo RL (1993) Developmental expression of the syndecans: possible function and regulation. Dev Suppl 119:205–212

Bespalov MM, Sidorova YA, Tumova S, Ahonen-Bishopp A, Magalhaes AC, Kulesskiy E, Paveliev M, Rivera C, Rauvala H, Saarma M (2011) Heparan sulfate proteoglycan syndecan-3 is a novel receptor for GDNF, neurturin, and artemin. J Cell Biol 192(1):153–169. https://doi.org/10.1083/jcb.201009136

Caldwell JH, Schaller KL, Lasher RS, Peles E, Levinson SR (2000) Sodium channel Na(v)1.6 is localized at nodes of ranvier, dendrites, and synapses. Proc Natl Acad Sci U S A 97(10):5616–5620. https://doi.org/10.1073/pnas.090034797

Chattopadhyay S, Shubayev VI (2009) MMP-9 controls Schwann cell proliferation and phenotypic remodeling via IGF-1 and ErbB receptor-mediated activation of MEK/ERK pathway. Glia 57(12):1316–1325. https://doi.org/10.1002/glia.20851

Clausen TM, Pereira MA, Al Nakouzi N, Oo HZ, Agerbaek MO, Lee S, Orum-Madsen MS, Kristensen AR, El-Naggar A, Grandgenett PM, Grem JL, Hollingsworth MA, Holst PJ, Theander T, Sorensen PH, Daugaard M, Salanti A (2016) Oncofetal chondroitin sulfate glycosaminoglycans are key players in integrin signaling and tumor cell motility. Mol Cancer Res 14(12):1288–1299. https://doi.org/10.1158/1541-7786.MCR-16-0103

Couchman JR (2003) Syndecans: proteoglycan regulators of cell-surface microdomains? Nat Rev Mol Cell Biol 4(12):926–937. https://doi.org/10.1038/nrm1257

Coulson-Thomas VJ (2016) The role of heparan sulphate in development: the ectodermal story. Int J Exp Pathol 97(3):213–229. https://doi.org/10.1111/iep.12180

Dufour A, Zucker S, Sampson NS, Kuscu C, Cao J (2010) Role of matrix metalloproteinase-9 dimers in cell migration: design of inhibitory peptides. J Biol Chem 285(46):35944–35956. https://doi.org/10.1074/jbc.M109.091769

Edwards TJ, Hammarlund M (2014) Syndecan promotes axon regeneration by stabilizing growth cone migration. Cell Rep 8(1):272–283. https://doi.org/10.1016/j.celrep.2014.06.008

Elfenbein A, Simons M (2013) Syndecan-4 signaling at a glance. J Cell Sci 126(Pt 17):3799–3804. https://doi.org/10.1242/jcs.124636

Ferguson TA, Muir D (2000) MMP-2 and MMP-9 increase the neurite-promoting potential of schwann cell basal laminae and are upregulated in degenerated nerve. Mol Cell Neurosci 16(2):157–167. https://doi.org/10.1006/mcne.2000.0859

Fukuda T, Kusuhara H, Nakagoshi T, Isogai N, Sueyoshi Y (2018) A basic fibroblast growth factor slow-release system combined to a biodegradable nerve conduit improves endothelial cell and Schwann cell proliferation: A preliminary study in a rat model. Microsurgery 38(8):899–906. https://doi.org/10.1002/micr.30387

Gao X, Wang Y, Chen J, Peng J (2013) The role of peripheral nerve ECM components in the tissue engineering nerve construction. Rev Neurosci 24(4):443–453. https://doi.org/10.1515/revneuro-2013-0022

Garber M, Grabherr MG, Guttman M, Trapnell C (2011) Computational methods for transcriptome annotation and quantification using RNA-seq. Nat Methods 8(6):469–477. https://doi.org/10.1038/nmeth.1613

Gardiner DM (2017) Regulation of regeneration by heparan sulfate proteoglycans in the extracellular matrix. Regen Eng Transl Med 3(3):192–198. https://doi.org/10.1007/s40883-017-0037-8

Goutebroze L, Carnaud M, Denisenko N, Boutterin MC, Girault JA (2003) Syndecan-3 and syndecan-4 are enriched in Schwann cell perinodal processes. BMC Neurosci 4:29. https://doi.org/10.1186/1471-2202-4-29

Henry MA, Freking AR, Johnson LR, Levinson SR (2007) Sodium channel Nav1.6 accumulates at the site of infraorbital nerve injury. BMC Neurosci. 8:56. https://doi.org/10.1186/1471-2202-8-56

Hsueh YP, Sheng M (1999) Regulated expression and subcellular localization of syndecan heparan sulfate proteoglycans and the syndecan-binding protein CASK/LIN-2 during rat brain development. J Neurosci 19(17):7415–7425

Jordanova A, Thomas FP, Guergueltcheva V, Tournev I, Gondim FA, Ishpekova B, De Vriendt E, Jacobs A, Litvinenko I, Ivanova N, Buzhov B, De Jonghe P, Kremensky I, Timmerman V (2003) Dominant intermediate Charcot-Marie-Tooth type C maps to chromosome 1p34-p35. Am J Hum Genet 73(6):1423–1430. https://doi.org/10.1086/379792

Katz E, Stoler O, Scheller A, Khrapunsky Y, Goebbels S, Kirchhoff F, Gutnick MJ, Wolf F, Fleidervish IA (2018) Role of sodium channel subtype in action potential generation by neocortical pyramidal neurons. Proc Natl Acad Sci U S A 115(30):E7184–E7192. https://doi.org/10.1073/pnas.1720493115

Kim Y, Remacle AG, Chernov AV, Liu H, Shubayev I, Lai C, Dolkas J, Shiryaev SA, Golubkov VS, Mizisin AP, Strongin AY, Shubayev VI (2012) The MMP-9/TIMP-1 axis controls the status of differentiation and function of myelin-forming Schwann cells in nerve regeneration. PLoS ONE 7(3):e33664. https://doi.org/10.1371/journal.pone.0033664

Leterrier C, Brachet A, Fache MP, Dargent B (2010) Voltage-gated sodium channel organization in neurons: protein interactions and trafficking pathways. Neurosci Lett 486(2):92–100. https://doi.org/10.1016/j.neulet.2010.08.079

Liao WC, Wang YJ, Huang MC, Tseng GF (2013) Methylcobalamin facilitates collateral sprouting of donor axons and innervation of recipient muscle in end-to-side neurorrhaphy in rats. PLoS ONE 8(9):e76302. https://doi.org/10.1371/journal.pone.0076302

Liu CH, Chang HM, Tseng TJ, Lan CT, Chen LY, Youn SC, Lee JJ, Mai FD, Chou JF, Liao WC (2016) Redistribution of Cav21 channels and calcium ions in nerve terminals following end-to-side neurorrhaphy: ionic imaging analysis by TOF-SIMS. Histochem Cell Biol 146(5):599–608. https://doi.org/10.1007/s00418-016-1470-3

Liu CH, Chang HM, Wu TH, Chen LY, Yang YS, Tseng TJ, Liao WC (2017) Rearrangement of potassium ions and Kv1.1/Kv1.2 potassium channels in regenerating axons following end-to-end

neurorrhaphy: ionic images from TOF-SIMS. Histochem Cell Biol 148(4):407–416. https://doi.org/10.1007/s00418-017-1570-8
Mackenzie F, Ruhrberg C (2012) Diverse roles for VEGF-A in the nervous system. Development 139(8):1371–1380. https://doi.org/10.1242/dev.072348
Manon-Jensen T, Itoh Y, Couchman JR (2010) Proteoglycans in health and disease: the multiple roles of syndecan shedding. FEBS J 277(19):3876–3889. https://doi.org/10.1111/j.1742-4658.2010.07798.x
Marchionini DM, Lehrmann E, Chu Y, He B, Sortwell CE, Becker KG, Freed WJ, Kordower JH, Collier TJ (2007) Role of heparin binding growth factors in nigrostriatal dopamine system development and Parkinson's disease. Brain Res 1147:77–88. https://doi.org/10.1016/j.brainres.2007.02.028
Marquardt LM, Ee X, Iyer N, Hunter D, Mackinnon SE, Wood MD, Sakiyama-Elbert SE (2015) Finely tuned temporal and spatial delivery of GDNF promotes enhanced nerve regeneration in a long nerve defect model. Tissue Eng Part A 21(23–24):2852–2864. https://doi.org/10.1089/ten.TEA.2015.0311
Matthews HK, Marchant L, Carmona-Fontaine C, Kuriyama S, Larrain J, Holt MR, Parsons M, Mayor R (2008) Directional migration of neural crest cells in vivo is regulated by Syndecan-4/Rac1 and non-canonical Wnt signaling/RhoA. Development 135(10):1771–1780. https://doi.org/10.1242/dev.017350
Meneghetti MC, Hughes AJ, Rudd TR, Nader HB, Powell AK, Yates EA, Lima MA (2015) Heparan sulfate and heparin interactions with proteins. J R Soc Interface 12(110):0589. https://doi.org/10.1098/rsif.2015.0589
Mitsou I, Multhaupt HAB, Couchman JR (2017) Proteoglycans, ion channels and cell-matrix adhesion. Biochem J 474(12):1965–1979. https://doi.org/10.1042/BCJ20160747
Oberlin C, Beal D, Leechavengvongs S, Salon A, Dauge MC, Sarcy JJ (1994) Nerve transfer to biceps muscle using a part of ulnar nerve for C5–C6 avulsion of the brachial plexus: anatomical study and report of four cases. J Hand Surg Am 19(2):232–237. https://doi.org/10.1016/0363-5023(94)90011-6
Park PW (2018) Isolation and functional analysis of syndecans. Methods Cell Biol 143:317–333. https://doi.org/10.1016/bs.mcb.2017.08.019
Prince RN, Schreiter ER, Zou P, Wiley HS, Ting AY, Lee RT, Lauffenburger DA (2010) The heparin-binding domain of HB-EGF mediates localization to sites of cell-cell contact and prevents HB-EGF proteolytic release. J Cell Sci 123(Pt 13):2308–2318. https://doi.org/10.1242/jcs.058321
Quintes S, Goebbels S, Saher G, Schwab MH, Nave KA (2010) Neuron-glia signaling and the protection of axon function by Schwann cells. J Peripher Nerv Syst 15(1):10–16. https://doi.org/10.1111/j.1529-8027.2010.00247.x
Sarrazin S, Lamanna WC, Esko JD (2011) Heparan sulfate proteoglycans. Cold Spring Harb Perspect Biol. https://doi.org/10.1101/cshperspect.a004952
Schlosshauer B, Muller E, Schroder B, Planck H, Muller HW (2003) Rat Schwann cells in bioresorbable nerve guides to promote and accelerate axonal regeneration. Brain Res 963(1–2):321–326. https://doi.org/10.1016/s0006-8993(02)03930-6
Susuki K, Chang KJ, Zollinger DR, Liu Y, Ogawa Y, Eshed-Eisenbach Y, Dours-Zimmermann MT, Oses-Prieto JA, Burlingame AL, Seidenbecher CI, Zimmermann DR, Oohashi T, Peles E, Rasband MN (2013) Three mechanisms assemble central nervous system nodes of Ranvier. Neuron 78(3):469–482. https://doi.org/10.1016/j.neuron.2013.03.005
Wang CC, Yen JH, Cheng YC, Lin CY, Hsieh CT, Gau RJ, Chiou SJ, Chang HY (2017) Polygala tenuifolia extract inhibits lipid accumulation in 3T3-L1 adipocytes and high-fat diet-induced obese mouse model and affects hepatic transcriptome and gut microbiota profiles. Food Nutr Res 61(1):1379861. https://doi.org/10.1080/16546628.2017.1379861
Webber C, Zochodne D (2010) The nerve regenerative microenvironment: early behavior and partnership of axons and Schwann cells. Exp Neurol 223(1):51–59. https://doi.org/10.1016/j.expneurol.2009.05.037